JACS
JOURNAL OF THE AMERICAN CHEMICAL SOCIETY
Article
pubs.acs.org/JACS

Highly Stable, Anion Conductive, Comb-Shaped Copolymers for Alkaline Fuel Cells

Nanwen Li,[†] Yongjun Leng,[‡] Michael A. Hickner,*[,†] and Chao-Yang Wang[‡]

[†]Department of Materials Science and Engineering, The Pennsylvania State University, University Park, Pennsylvania 16802, United States

[‡]Electrochemical Engine Center, Department of Mechanical and Nuclear Engineering, The Pennsylvania State University, University Park, Pennsylvania 16802, United States

ABSTRACT: To produce an anion-conductive and durable polymer electrolyte for alkaline fuel cell applications, a series of quaternized poly(2,6-dimethyl phenylene oxide)s containing long alkyl side chains pendant to the nitrogen-centered cation were synthesized using a Menshutkin reaction to form comb-shaped structures. The pendant alkyl chains were responsible for the development of highly conductive ionic domains, as confirmed by small-angle X-ray scattering (SAXS). The comb-shaped polymers having one alkyl side chain showed higher hydroxide conductivities than those with benzyltrimethyl ammonium moieties or structures with more than one alkyl side chain per cationic site. The highest conductivity was observed for comb-shaped polymers with benzyldimethylhexadecyl ammonium cations. The chemical stabilities of the comb-shaped membranes were evaluated under severe, accelerated-aging conditions, and degradation was observed by measuring IEC and ion conductivity changes during aging. The comb-shaped membranes retained their high ion conductivity in 1 M NaOH at 80 °C for 2000 h. These cationic polymers were employed as ionomers in catalyst layers for alkaline fuel cells. The results indicated that the C-16 alkyl side chain ionomer had a slightly better initial performance, despite its low IEC value, but very poor durability in the fuel cell. In contrast, 90% of the initial performance was retained for the alkaline fuel cell with electrodes containing the C-6 side chain after 60 h of fuel cell operation.

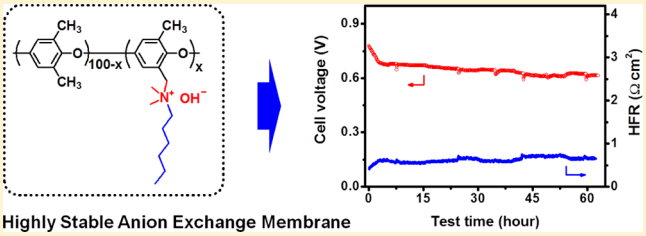

INTRODUCTION

Fuel cells are efficient energy conversion devices that generate electric power from energy-dense chemical fuels and have been attracting attention as a clean energy technology.[1−3] The most widespread low-temperature fuel cell technologies are based on sulfonated polymer membranes to separate the oxidant and fuel chambers and conduct protons between the anode and cathode of the cell.[4−6] These proton exchange membrane fuel cells (PEMFC) principally employ Nafion, a product from DuPont, as the sulfonated polymeric proton conductor. PEMFCs require platinum or other precious metal-based catalysts because these are the only types of metal catalysts stable under the low pH and electrochemical conditions of an operating cell. The expensive Pt-based catalysts, combined with perfluorinated membranes and corrosion-resistant cell hardware increase the cost of PEMFC devices beyond what is currently commercially viable.[7,8]

Alkaline fuel cells (AFCs) have received significant interest in recent years relative to acidic fuel cells,[9−14] because of advantages when operating under alkaline conditions, which include enhancement of the electrode reaction kinetics, especially at the cathode, and the catalysts are not subjected to corrosion at high pH.[9,12,13] Consequently, non-noble metals or inexpensive metal oxides can be used as catalysts to greatly reduce the cost of the device.[13−16] In addition, high energy density liquids and gases such as ethanol, hydrazine, and ammonia can be adopted as fuels.[17,18] Alkaline fuel cells were initially conceived with liquid basic electrolytes containing alkali metal cations, such as sodium hydroxide or potassium hydroxide. Recently, polymers with tethered organic cations have been demonstrated as solid polymer anion-exchange membranes (AEMs) for alkaline fuel cells. These hydroxide conductive organic cations have been obtained by introducing quaternary ammonium (QA),[19,20] guandinium,[22,23] or phosphonium groups[24] using chloromethylation of aromatic rings or bromination on the benzylic methyl groups of the polymers, followed by the Menshutkin reaction with a tertiary amine, pentamethylguanidine, or tertiary phosphine. Various polymer backbone structures—poly(olefin)s,[25] poly(styrene)s,[26−28] poly(phenylene oxide)s,[29,30] poly(phenylene)s,[31] poly(arylene ether)s[19−24]—have been investigated recently, displaying a wide range of ion conductivities. While all of these systems demonstrated reasonable properties as AEMs and established the feasibility for alkaline membrane electrode assemblies, conductivity improvement and alkaline stability enhancement are still the major challenges in the development of AEMs.[32−39] Another significant problem for AMFCs is the lack of a soluble ionomer to be used in the catalyst layer with good solubility in low-boiling point, water-miscible solvents such as ethanol or *n*-

Received: April 12, 2013
Published: May 30, 2013

   dx.doi.org/10.1021/ja403671u | J. Am. Chem. Soc. 2013, 135, 10124−10133

propanol/2-propanol. Ionomers cast from these easy-to-process solutions must have high hydroxide conductivity and alkaline stability after solidification to build an efficient three-phase catalyst boundary and thus drastically improve the utilization of the catalyst particles and reduce the catalyst layer and interfacial resistance.[24]

We have developed a series of cationic poly(2,6-dimethyl-phenylene oxide) (PPO) AEMs which displayed improved anion conductivities, substantial alkaline stability, and advantageous properties for incorporation as catalyst ionomers in fuel cell devices.[30] One of our most important findings is that introducing one long alkyl chain of up to 16 carbon atoms pendant to the cationic center formed comb-shaped structures which induced hydrophilic−hydrophobic separation, and thus enhanced the ionic conductivities of these materials. Moreover, the long alkyl side chain could significantly mitigate water swelling of the membrane and reduce the nucleophilic attack of water or hydroxide at the quaternary ammonium (QA) moieties resulting in good alkaline stability of the PPO ionomers. The improved stability of these types of cations has been supported by computational calculations using model compounds which revealed that attachment of quaternary ammonium groups to the polymer backbone having an alkyl spacer of >3 carbon atoms can lead to improved alkaline stability of the cation.[39,40] Recently, Hibbs and co-workers reported a similar stability result for a poly(phenylene) backbone with trimetylalkylammonium cations attached by a hexamethylene spacer.[41] Although the comb-shaped PPO membranes showed promising properties as AEMs, poor mechanical properties were observed for high IEC (>2.0 meq/g) membranes probably due to the poor compatibility between long alkyl side chain and PPO backbone. We therefore tuned the number and length of alkyl side chains to develop a new system that would support high IEC values and thus high hydroxide conductivity, while retaining other good material properties, including hydroxide stability. A detailed investigation on the properties of quaternary-ammonium containing PPOs with different length alkyl side chains was performed. Their ionic conductivities, microphase-separated structure, and alkaline stability are described and compared to those of cationic PPOs with tethered benzyltrimethyl ammonium cations. The AMFC H_2/O_2 fuel cell performance using the comb-shaped PPO ionomers in the catalyst layer have further been demonstrated.

EXPERIMENTAL SECTION

Materials. Poly(2,6-dimethyl phenylene oxide) was obtained from Sigma-Aldrich and dried under vacuum at room temperature overnight. *N,N*-Dimethylhexylamine, *N,N*-dimethyldecylamine, *N,N*-dimethylhexadecylamine, *N*-methyldihexylamine, trihexylamine, *N*-bromosuccinimide, and 2,2′-azobis(2-methylpropionitrile) were purchased from Sigma-Aldrich and used without further purification. The brominated PPO polymers with different degrees of bromination (DB) ranging from 20 to 160% were prepared according to the literature.[30]

Polymer Synthesis and Membrane Preparation. Brominated PPO with a DB of 0.4 (1.5 g, 10 mmol) was dissolved in 20 mL of NMP. Subsequently, *N,N*-dimethylhexylamine (DMHA) (1.4 g, 15 mmol) was added. The mixture was stirred for 48 h at room temperature. The solution was filtered and then cast onto a flat glass plate. The cast solution was dried at 80 °C for 12 h to obtain a ductile membrane of **C6D40**, where the C6 refers to the length of alkyl chain and the D40 refers to the degree of bromination, where 40 refers to 0.4 bromomethyl groups per PPO repeat unit, on average. The film was dried further under vacuum at 80 °C for 20 h. The membranes in the bicarbonate form were achieved by exchanging the bromine form membranes with sodium bicarbonate followed by extensive rinsing to remove the excess salt. The **C6D40** membranes were treated in 1 N NaOH at room temperature for 48 h to obtain the hydroxide conductive membranes. The samples were then washed thoroughly and immersed in deionized water that was degassed and blanketed with flowing Ar to remove residual NaOH overnight to give a transparent, tough film.

All other membranes **CyDx**, **2CyDx**, and **3CyDx** (where the *y* is the number of carbon atoms of the alkyl side chain, and the *x*/100 refers to the degree of bromination) were prepared using similar procedures as described above.

Characterization and Measurements. ^{1}H NMR spectra were measured at 300 MHz on a Bruker AV 300 spectrometer using DMSO-d_6 as the solvent. The membranes in the bromide form were immersed in 100 mL of 0.1 M $NaNO_3$ standard for 24 h. The solutions were then titrated with a standardized $AgNO_3$ solution using K_2CrO_3 as an indicator to obtain the titrated gravimetric IEC values. Tensile measurements were performed with an Instron-1211 instrument at a crosshead speed of 1 mm/min at room temperature (25 °C) and 50% relative humidity (RH). All the samples were dried in vacuum at 60 °C for 10 h and equilibrated at 25 °C and 50% RH for at least 24 h before measurement.

Water uptake was measured after drying the membrane in hydroxide form at 60 °C under vacuum for 12 h. The dried membrane was immersed in water and periodically weighed on an analytical balance until a constant mass was obtained, giving the mass-based water uptake. Membrane densities and volumetric IEC_v (meq/cm^3) were determined according to previously reported methods[41] based on membrane water uptake using the following equation.

$$IEC_v = \frac{IEC_w}{\frac{1}{\rho_{polymer}} + \frac{WU\ (wt\%)}{100 \times \rho_{water}}} \quad (1)$$

where IEC_w is the gravimetric IEC (meq/g) and ρ (g/cm^3) is the density.

Conductivity (σ, S cm^{-1}) of each membrane sample (size: 1 cm × 4 cm) was obtained using $\sigma = d/L_sW_sR$ (d is the distance between reference electrodes, and L_s and W_s are the thickness and width of the membrane, respectively). The membrane impedance was measured over the frequency range from 100 mHz to 100 kHz by two-point probe alternating current (AC) impedance spectroscopy using an impedance/gain-phase analyzer (Solartron 1260A, Solartron Analytical, Farnborough Hampshire, ONR, UK). The hydroxide conductivity measurements under fully hydrated conditions in the longitudinal direction were carried out with the cell immersed in water which was degassed and blanketed with flowing Ar.

Small-angle X-ray scattering curves of unstained dry bicarbonate form membranes were obtained using a Rigaku (formerly Molecular Metrology) instrument equipped with a pinhole camera with an Osmic microfocus Cu K_α source and a parallel beam optic. Typical counting times for integration over a multiwire area detector were 1 h with typical membrane thicknesses on the order of 100 μm. Measurements were taken under vacuum at ambient temperature on dry samples. Scattering intensities were normalized for background scattering and beam transmission.

Fabrication of Membrane/Electrode Assemblies (MEA). A well-dispersed catalyst ink was prepared by mixing 46.4 wt % Pt/C catalysts (TKK, Japan) with deionized water, 1-propanol, and ionomer solution (5 wt % polymer in 1-propanol) using magnetic stirring and ultrasonication. To obtain a catalyst-coated substrate (CCS) for the electrodes, the as-prepared ink was coated onto the surface of SGL 25BC carbon paper (SGL group, Germany) using an air spray gun (Iwata, Japan). The Pt loading and ionomer content in the catalyst layer were 0.50−0.60 mg/cm^2 and ∼20 wt %, respectively. Anode CCS, A201 membrane (Tokuyama Corporation, Japan), and cathode CCS were assembled together in a cell fixture to form a membrane/electrode assembly (MEA). The electrode size was 2.25 cm × 2.25 cm (∼5 cm^2).

dx.doi.org/10.1021/ja403671u | J. Am. Chem. Soc. 2013, 135, 10124−10133

Scheme 1. Synthesis of Comb-Shaped CyDx Copolymers

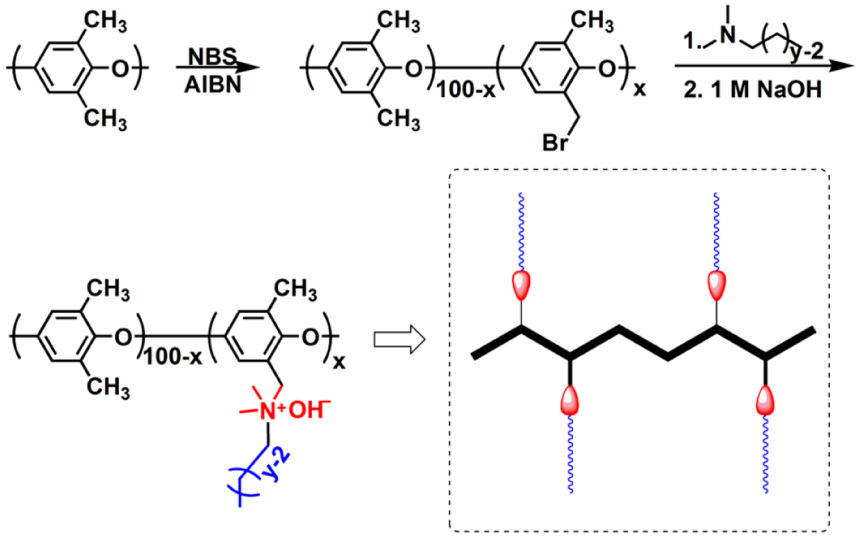

Table 1. IEC, Water Uptake, and Hydroxide Conductivity of BTMAx and Comb-Shaped CyDx Membranes

sample	IEC_w [a]	IEC_w [b]	IEC_w [c]	IEC_v	water uptake (wt %)[d]	λ	in-plane swelling (%)	conductivity (mS/cm)[d]
C6D20	1.34	1.33	1.31	1.24	10	4.2	2	10
C6D40	2.20	2.16	2.08	1.82	16	4.2	3	28
C6D60	2.81	2.82	2.75	1.06	150	30.3	200	43
C10D20	1.25	1.27	1.22	1.19	8	3.7	2	6
C10D40	1.97	1.86	1.88	1.74	12	3.5	2	12
C10D60	2.43	2.36	2.39	2.10	16	3.7	4	28
C16D20	1.13	1.09	1.08	1.07	7	3.7	2	6
C16D40	1.70	1.71	1.65	1.54	11	3.8	2	21
C16D60	2.01	1.98	1.92	1.72	14	4.1	3	30
BTMA20	1.39	1.42	1.37	1.17	20	8.0	5	6
BTMA30	2.10	2.04	2.03	1.28	59	16.0	13	16
BTMA40	2.66	2.59	2.64	1.06	130	27.2	180	24

[a]Calculated from the copolymer composition and the degree of bromination. [b]Calculated from ^{1}H NMR. [c]Titrated values. [d]Measured at room temperature in water.

Fuel Cell Performance Evaluation. Fuel cell testing was conducted with a commercial fuel cell testing system (Teledyne, U.S.A.). The 5 cm^2 MEAs were mounted in a 2.25 cm × 2.25 cm test fixture containing two graphite blocks with machined single serpentine flow channels and two gold-coated current collector plates. The fuel cell performance was measured at 50 °C. The anode/cathode humidifier temperatures were controlled to be 2−3 °C higher than the cell temperature in order to achieve full humidification (RH = 100%). Fully humidified hydrogen was supplied to the anode at 200−2000 sccm as indicated in the data, while fully humidified oxygen was supplied to the cathode at 200−2000 sccm. The MEA was activated by operating at high current density (potentiostatic cell discharge at 100 mV) until the current density increased to a maximum and became constant after 30 min to 1 h. After full activation, the fuel cell polarization curve was measured under galvanostatic mode, i.e. holding the fuel cell at serial constant currents (for example, 50, 100, and 250 mA/cm^2, etc.) for 3 min. The cell voltage as a function of current density was recorded using fuel cell testing software. For the durability testing at 50 °C, fully humidified hydrogen was supplied into the anode with a flow rate of 500 sccm, while fully humidified oxygen was supplied into the cathode with a flow rate of 200 sccm. A current density of 100 mA/cm^2 was applied to the fuel cell, and cell voltage and high frequency resistance (HFR) as a function of test time were recorded.

RESULTS AND DISCUSSION

Synthesis and Characterization of Comb-Shaped CyDx Ionomers. First, the brominated poly(2,6-dimethyl phenylene oxide) (PPO) with different degrees of bromination (DB) at the benzyl position were prepared according to previous reports using *N*-bromosuccinimide and azobisisobutyronitrile. The highest DB of 1.6 (an average of 1.6 bromomethyl groups per PPO repeat unit) could be achieved in a refluxing chlorobenzene solution for 3 h. Then, a series of comb-shaped quaternized PPOs (**CyDx**) with varying degrees of bromination (DB, *x*) and side-chain length (*y*, 6−16) were synthesized using the Menshutkin reaction with *N*,*N*-dimethylhexylamine, *N*,*N*-dimethyldecylamine, or *N*,*N*-dimethyl-1-hexadecylamine (Scheme 1). The DB was set at 0.2, 0.4, and 0.6 to obtain samples with calculated ion-exchange capacity (IEC_w) ranging from 1.13 to 2.81 meq/g (Table 1). Casting from NMP solution gave tough and ductile brown-colored transparent membranes with a thickness of ∼70 μm. The obtained membranes exhibited excellent solubility in pure methanol, ethanol, and *n*-propanol. However, the **CyDx** ionomers were insoluble in pure water, even at 80 °C, suggesting that this type of polymer can be used in the catalyst layer without losses arising from solubility. Our original intention was to prepare comb-shaped **CyDx** membranes

dx.doi.org/10.1021/ja403671u | J. Am. Chem. Soc. 2013, 135, 10124−10133

with very high IEC_w above 3.0 meq/g (the DB would be more than 0.8) using *N,N′*-dimethylalkylamines. In spite of numerous attempts, the high IEC copolymers displayed very poor film-forming ability. After solvent evaporation during membrane casting, the samples were broken into small pieces and became completely opaque. The inability to obtain flexible and tough membranes may be attributed to the incompatibility of the long alky chain and aromatic PPO backbone and the decreased interaction between polymer backbones as a result of the numerous pendant long alkyl chains.

The comb-shaped **CyDx** cationic copolymers in bromine salt form were characterized by ^{1}H NMR spectroscopy. The disappearance of the proton resonance from the bromobenzyl moiety as a sharp peak at 4.3 ppm along with the appearance of peaks for the alkyl chains at 0.5−1.8 ppm and 3.0 ppm indicated that the quaternary ammonium group was formed successfully. A broad resonance from 4.3 ppm to 4.51 ppm was observed, which could be assigned to the two benzylic protons, H6 (Figure 1), probably due to the deshielding effect from the

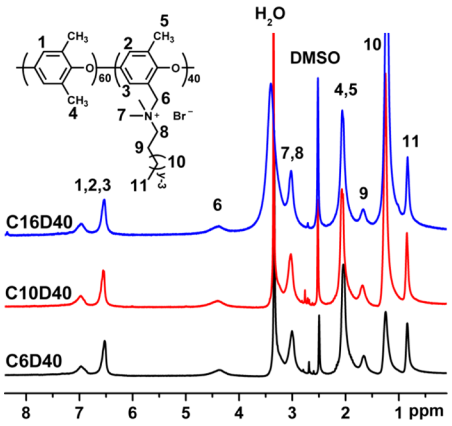

Figure 1. ^{1}H NMR of comb-shaped **C6D40**, **C10D40**, and **C16D40** in bromine form in DMSO-d_6.

quaternary ammonium salt. The integral ratio of the methyl and methylene protons, H9, H10, and H11, at 0.5−1.8 ppm (or protons H7 and H8 at 3.0 ppm) to aromatic proton peaks at 6.5−7.2 ppm indicated that the quaternization reaction was quantitative. The ion-exchange capacities (IEC_w) of the **CyDx** membranes were calculated to be from 1.09 to 2.82 meq/g from the integral ratios, which were in good agreement with the calculated values from the copolymer compositions and the degree of brominations, suggesting further that complete quaternization of the bromomethyl groups occurred, Table 1. Despite the presence of overlapping peaks, these IEC_w values from ^{1}H NMR are similar to the values determined from titration with errors on the order of ±10%.

Morpholigical Characterization of CyDx Membranes. We hypothesized that the hydrophilic polymer backbone (PPO) was immiscible with the hydrophobic aliphatic grafted side chain, thus driving comb-shaped PPOs to self-assemble and form nanoscale ionic domains. The SAXS profiles of four different membranes based on PPO copolymers are shown in Figure 2. Three samples were based on the alkyl side chains C6, C10, and C16, and one sample was based on the benzyltrimethyl ammonium cation (**BTMA20**). In gereral, the characteristic separation length between the ion-rich domains in ionomers can be observed in terms of the values of q corresponding to the so-called ionomer peak. As seen in Figure

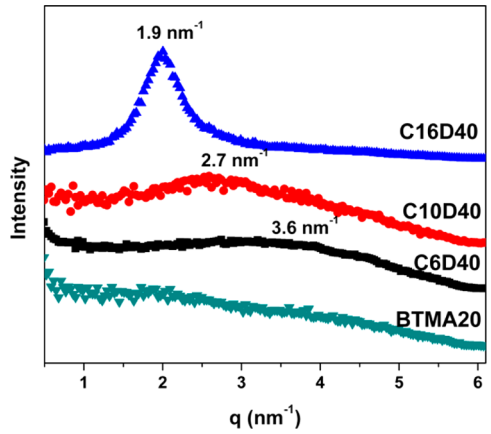

Figure 2. SAXS profiles of dry polymer membranes in bicarbonate form.

2, no ionomer peak was observed for the conventional **BTMA20** membrane without an alkyl side chain attached to the quaternary ammonium center. The SAXS data indicated no characteristic phase separation for such membranes based on trimethylamine. By replacing one of the methyl groups with an alkyl chain, the hydrophobicity of side chain and the hydrophilic−hydrophobic separation can be expected to be enhanced, as compared to conventionally quaternized polymers. Thus, the conditions for ionic domain formation and phase separation should be improved. By comparing the SAXS traces in Figure 2 of membrane **BTMA20** and the membranes based on the comb-shaped copolymers with one long alkyl side chain, it is clear that the latter polymers showed obvious characteristic ionomer peaks, indicating the formation of nanophase separation with ionic domains. The relatively narrow peak profiles of membranes based on **C16D40** with the longest hexadecyl side chain suggested that the ionic domains formed a distinct, well-separated phase. The large width of the peaks of **C10D40** and **C6D40** with relatively short alkyl side chains indicated weak separation between the two components and no long-range order. The lack of a second order scattering peak for all membranes suggests that the arragnement of the phase separated domins is only locally correlated, and no long-range ordered structures formed in these materials. Moreover, as seen from the profiles of the comb-shaped **CyDx** membranes in Figure 2, the q values of the ionomer peak shifted to higher values as the length of alkyl chain decreased. The corresponding periodic structure with length scale d values ($d = 2\pi/q$) were 3.3 nm, 2.3 and 1.7 nm for **C16D40**, **C10D40** and **C6D40** membranes, respectively, which roughly corresponds to the length of the extended aliphatic side chains. This finding is of great interest because it showed that phase separated systems may be achieved with quaternized aromatic polymers membranes with proper molecular design. As will be shown below, the self-assembled structure visible in the SAXS experiments had a strong influence on water uptake and ionic transport.

Water Uptake Behavior of CyDx Membranes. Table 1 lists the water uptake (WU) of **CyDx** membranes at 20 °C in liquid water compared to **BTMAx** membranes. As expected, higher gravimetric IEC_w membranes absorbed more water due to their increased ion content. As shown in Figure 3a, the comb-shaped **CyDx** membranes with one long alkyl chain showed much lower water uptake than that of **BTMAx** membranes based on trimethylamine, thus exhibiting lower

dx.doi.org/10.1021/ja403671u | J. Am. Chem. Soc. 2013, 135, 10124−10133

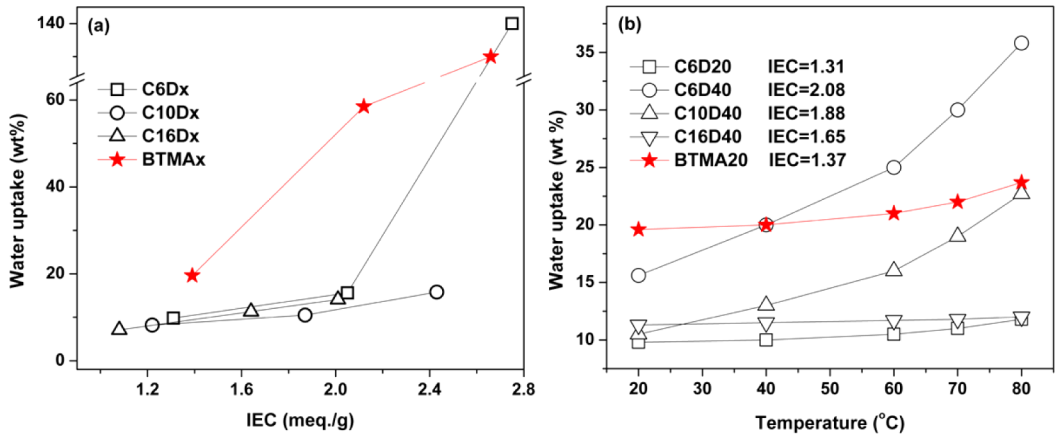

Figure 3. Liquid water uptake of membranes as a function of (a) IEC_w and (b) temperature.

dimensional swelling behavior (Table 1, in-plane swelling). The number of absorbed water molecules per quaternary ammonium (QA) group, the hydration number or λ, was calculated to be lower than 5 except for the **C6D60** membrane, because it swelled excessively in water due to its high IEC_w value. These hydration values are lower than that of the **BTMAx** samples ($\lambda > 7$). It is assumed that the long alkyl chain showed strong hydrophobicity which restricted the water absorption of the comb-shaped copolymers. Similar water absorption behavior which depended on their IEC_w values were observed for all the comb-shaped membranes in spite of their different alkyl chain lengths, Figure 3a. However, the length of the alkyl chain had an obvious influence on the water uptake at high temperature. Figure 3b shows the temperature dependence of the water uptake when the membranes were exposed to liquid water. Although all of the membranes exhibited increases in water uptake with temperature, the copolymer **C16D40** with the longest alkyl chain displayed a much lower increase in water uptake with temperature compared to **C6D40** and **C10D40** membranes. For example, comb-shaped **C6D40** with one hexyl side chain showed 16 wt % water uptake in water at room temperature, whereas the water uptake increased to 32 wt % at 80 °C. However, similar water absorption behavior was observed at all temperatures for the **C16D40** membrane which had the longest hexadecyl side chain. These results indicated that the hydrophobicity of hexadecyl chain could restrict the water absorption of membranes more efficiently at higher temperature. Moreover, the morphological structure with well-defined nanophase separation is also believed to be responsible for the lower swelling ratio: the formation of more-ordered nanoionic domains allowed for a more continuous and cohesive hydrophobic matrix that opposed the weakening of the polymer matrix at high temperature.

For a more telling comparison of the water uptake among the comb-shaped **CyDx** membranes, the volumetric IEC (IEC_v, meq/cm^3), which is defined as the molar concentration of QA groups per unit volume of the hydrated material, is a useful parameter for the detailed comparison of the water uptake and hydrated ion content among the membranes. As anticipated from the water uptake results shown in Figure 3, lower volumetric IEC_v were found for the **BTMAx** membranes after immersion in liquid water than for the samples containing one long alkyl chain. Normally, the IEC_v of membranes increases with increasing IEC_w. IEC_v increaes with more ions tethered to the chain as long as the water uptake is not excessive and dilution effects have not set in. For example, the IEC_v of **C10Dx** membranes with a C10 alkyl chain increased from 1.19 to 2.10 meq/cm^3 as IEC_w increased from 1.22 to 2.39 meq/g. However, excessive water uptake results in high swelling of membranes and dilution of the ions after equilibration with water. As shown in Figure 4, the **C6D60** and **BTMA40** membranes have high IEC_w values but low IEC_v due to the excessive swelling when exposed to liquid water leading to a loss in their mechanical properties. Although the high IEC membrane (up to 3.0 meq/g) with C6 or C10 alkyl chain could not be obtained as discussed above, the copolymers did not show excessive swelling in liquid water suggesting the long alkyl chain restricted the water absorption more effectively.

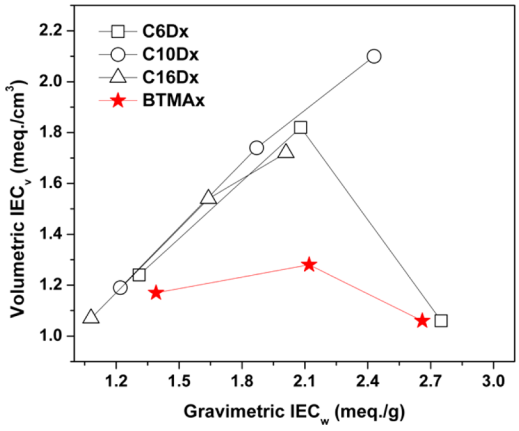

Figure 4. Volumetric IEC_v of comb-shaped copolymer **CyDx** and **BTMAx** membranes in water at RT as a function of gravimetric IEC_w.

Ionic Transport in CyDx Membranes. Similar to the water uptake, the hydroxide conductivity of the comb-shaped membranes increased with increasing IEC_w because of the increase in the water content which increased the local mobility of water and induced long-range ionic domain percolation. When comparing the hydroxide conductivity of comb-shaped **CyDx** and **BTMAx** membranes, the three comb-shaped membranes showed much higher conductivity compared to **BTMAx** membranes under the same conditions. For example, the **C6D60** membrane with IEC_w = 2.75 meq/g showed the highest conductivity (43 mS/cm), which was almostly two times higher than that of the **BTMA40** membrane (24 mS/cm) with IEC_w of 2.66 meq/g. Phase separation was driven by the

dx.doi.org/10.1021/ja403671u | J. Am. Chem. Soc. 2013, 135, 10124−10133

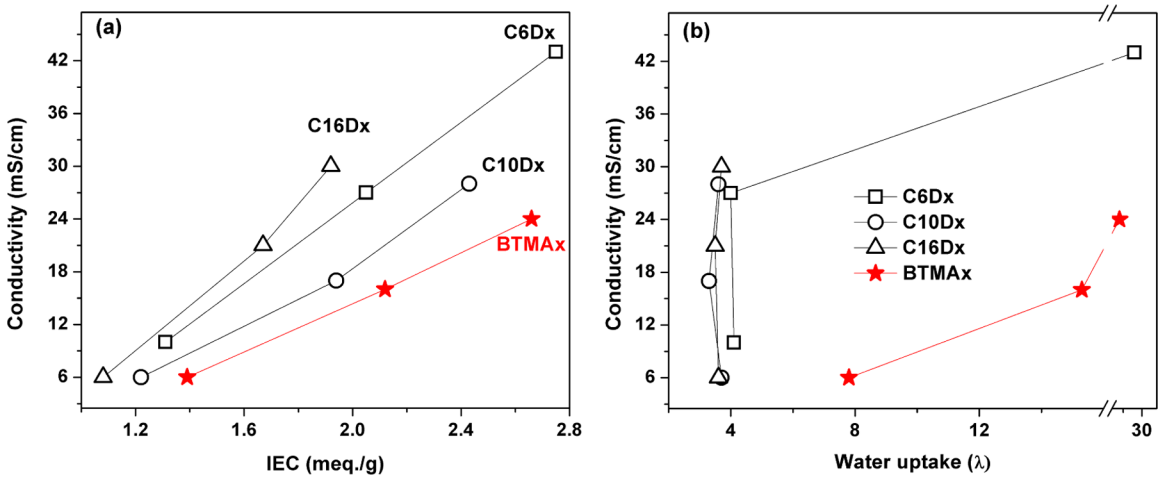

Figure 5. Hydroxide conductivity of **CyDx** and **BTMAx** at 20 °C as a function of (a) ion-exchange capacity and (b) the absorbed water molecules per QA-group (λ value).

alkyl chains attached to the quaternary ammonium centers, thereby resulting in the formation of ionic domains for effective hydroxide transport, as observed in the SAXS studies. As demonstrated by McGrath and co-workers, the continuity of nanoscale domains is critical to efficient proton transport in sulfonated polymers.[42] For our copolymers, the phase-separated ionic domains provided by comb polymer structures clearly enhances hydroxide conductivity by several times compared with conventional benzyltrimethyl-based AEMs. It is important to point out that the comb-shaped **CyDx** membranes showed a lower water uptake but considerably higher hydroxide conductivity than the **BTMAx** membranes. Overall, the comb-shaped **CyDx** membranes located at the left-hand part of Figure 5b indicate high hydroxide conductivity but lower hydration (λ value).

After normalizing the membrane hydroxide conductivity on the basis of the water volume fraction, the effective hydroxide conductivity in the water channels, σ', which indicates the efficiency of the water in the membrane for transport of hydroxide was obtained. The comb-shaped **CyDx** membranes, especially having hexadecyl chains showed higher values of σ' than the corresponding **BTMAx** membranes in spite of their low water volume fraction, as shown in Figure 6. This result indicates that the well-developed microphase separation of comb-shaped copolymer membranes could efficiently utilize water to facilitate hydroxide transport. These results suggest that our concept to apply the comb-shaped structure with long alkyl chain is a strategy for improving AEM ionic conductivity, as already demonstrated for phase-separated PEMs.[44]

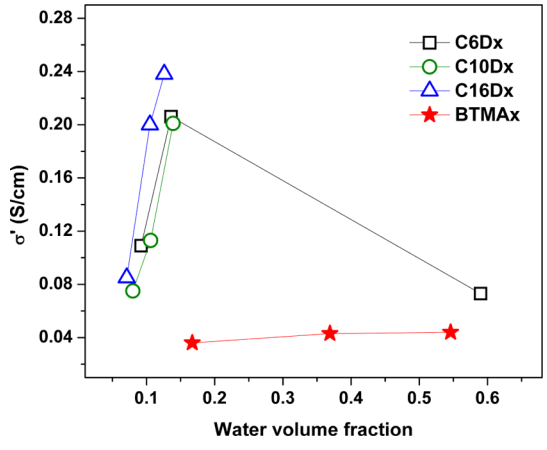

Figure 6. Water volume fraction dependence of the effective hydroxide conductivity (σ') in water at RT.

When comparing the hydroxide conductivity of comb-shaped membranes with different lengths of alkyl chains as shown in Figure 5a, the **C16Dx** membranes with the longest hexadecyl chain showed slightly higher conductivity than the other samples. For example, **C16D40** reached a hydroxide conductivity comparable to the **C10D60** membrane at room temperature, despite the lower IEC value of **C16D40**. It is believed that the highly phase-separated, uniform ionic domains of **C16Dx** membranes as probed in the SAXS studies could transport hydroxide ions more efficiently, thus yielding high hydroxide conductivities. This observation represents an unprecedented result in the molecular design of new anion-conducting platforms with optimized properties.

If carbonate and bicarbonate species should form in the membrane under operating conditions, the conductivities of our system are still significant. As shown in Figure 7a, all **CyDx** membranes displayed higher bicarbonate conductivity than that of **BTMAx** membranes. The **C6D40** membrane had a water uptake of 15.6 wt % (in OH^- form) and bicarbonate conductivity of 6.2 mS/cm at room temperature, which is much higher than that of the **BTMA20** membrane (2.1 mS/cm) in spite of the higher water uptake of the BTMA20 sample. Indeed, it has even been shown that power densities can be as good or better when CO_2 is introduced into an AFC due to improved electrode kinetics in the presence of carbonate.[45,46] The correlation between HCO_3^- conductivity and temperature for comb-shaped **CyDx** and **BTMAx** membranes is shown in Figure 7b. The conductivity steadily increased with temperature due to the enhanced water motion, and exhibited values of 8.7–17.2 mS cm^{-1} for **CyDx** membrane at 80 °C which is comparable to the previous reported values for AEMs having high water uptake (WU > 50 wt %).[19,25]

Alkaline Stability. The long-term stability of AEMs is generally of concern due to known degradation pathways for tetraalkylammonium ions under alkaline conditions[9,12] including β-hydrogen Hofmann elimination, direct nucleophilic substitution at an α-carbon, or nitrogen ylide formation. The alkaline stability of these AEMs was investigated in 1 M NaOH

dx.doi.org/10.1021/ja403671u | J. Am. Chem. Soc. 2013, 135, 10124–10133

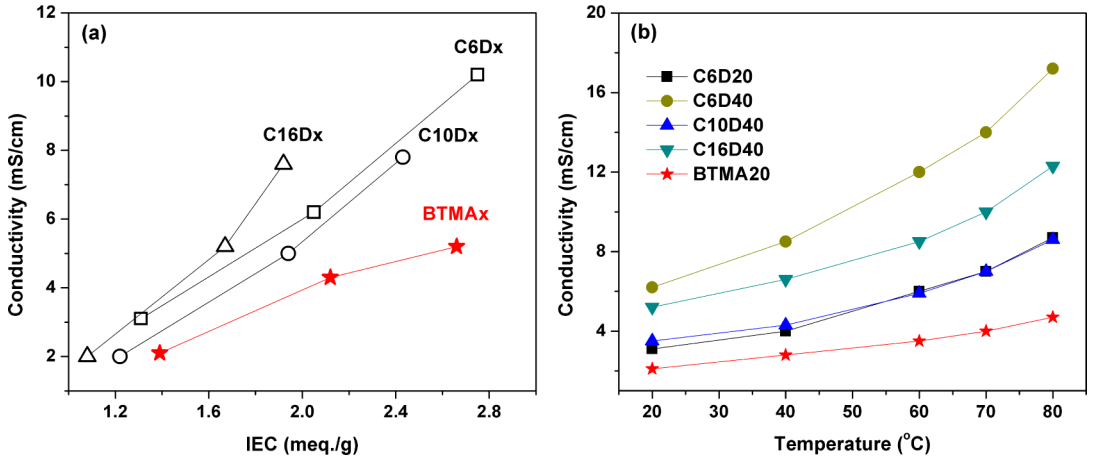

Figure 7. Bicarbonate conductivity of **CyDx** and **BTMAx** membranes as a function of (a) ion-exchange capacity at 20 °C and (b) temperature.

at 80 °C. The **BTMA20** membrane and other types of AEM structures showed poor alkaline stability at 80 °C[47] and the samples with tethered benzyltrimethyl ammonium cations broke into small pieces after 80 h stability testing. However, the comb-shaped **CyDx** membranes maintained acceptable mechanical properties even after 2000 h immersion in 1 M NaOH at 80 °C with replacement of the 1 M NaOH after every 7 days during the testing period. The **CyDx** samples did decrease in strength and showed some signatures of embrittlement over the long aging test, but the samples did not fail. The appearance of **C16D40** and **C10D40** membranes became opaque after several hundred hours, but the materials remained intact for the duration of the experiment. All of the **CyDx** membranes did not dissolve in hot water and experienced a weight loss of less than 15 wt % over the testing period. Although we could not obtain reduced viscosity and molecular weight changes due to the poor solubility of the aged **CyDx** samples, which possibly results from cross-linking during degradation, the samples retained reasonable mechanical properties while the BTMA20 membrane lost its mechanical properties completely after 80 h stability testing, likely as a result of chain scission, and broke into small pieces (data point goes below the *x*-axis − no measurement), as shown in Figure 8.

After an initial period of fast degradation over the first 200 h, the IEC values and bicarbonate conductivities of all membranes showed a slow, constant decline, Figure 9. This type of behavior might be expected if the alkyl chains are providing steric shielding of cationic domains in the membrane. Initial rapid degradation may occur for cations that are not incorporated in well-ordered alkyl regions. After these easy-to-access cations were degraded, degradation of sterically shielded cations may have occurred more slowly. It is assumed that the degradation of these materials was a result of typical direct nucleophilic substitution and/or β-hydrogen Hofmann elimination that occurs for quaternary ammonium moieties where the Hofmann elimination might also provide a pathway for the observed cross-linking and insolubility of the **CyDx** samples.[39,40] The bicarbonate conductivities of comb-shaped **CyDx** membranes remainted at ~80% of their initial values after the test of 2000 h while the conductivity of the **BTMA20** membane decreased rapidly to ~40% of the initial value after only 80 h (Figure 9a). This degradation behavior suggested that the comb-shaped membranes with one long alkyl side chain have much better alkaline stability than the **BTMA** membranes, and have

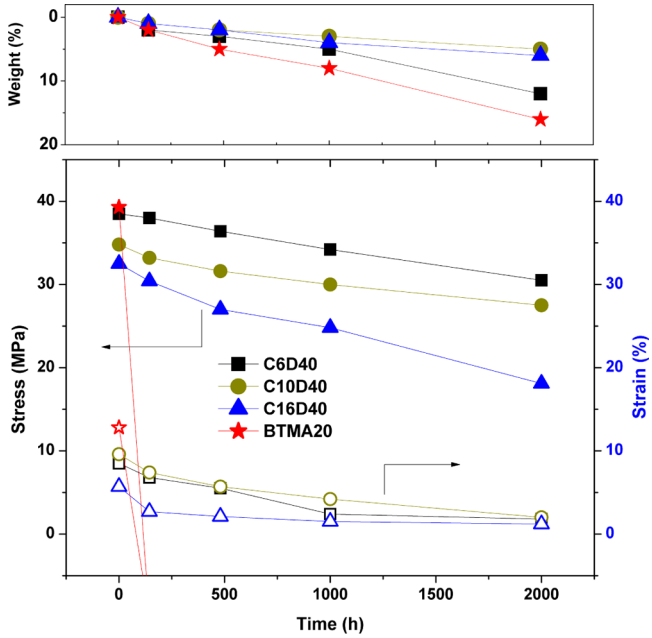

Figure 8. Decreases in mass and changes in mechanical properties of **CyDx** and **BTMAx** membranes as a function of time in 1 M NaOH at 80 °C.

sufficient long-term stability for AEM fuel cell applications. As shown in Figure 9b, the IEC value of comb-shaped **CyDx** membranes changed little during the stability testing, which further confirms their improved alkaline stability. This finding is supported by a recent computational study which predicts that *n*-alkyltrimethylammonium groups are more stable than BTMA when $n > 3$.[39,40] Although there are two β-hydrogen atoms around the quaternary ammounium groups in comb-shaped membranes in which the Hofmann elimination is probably the preferred decomposition pathway, the steric hindrance of the alkyl chains may hinder Hofmann elimination and protect the ammonium cations from being attacked by OH^-.

Quaternized PPO with Multiple Alkyl Side Chains. To further investigate the effect of alkyl side chains on the properties of AEMs, amines with two or three hexyl side chains (*N*-methyldihexylamine or trihexylamine) were employed in the Menshutkin reaction to obtain **2C6Dx** and **3C6Dx** membranes by a synthetic process similar to that described above (Scheme 2). Herein, the multihexyl chain was introduced

dx.doi.org/10.1021/ja403671u | J. Am. Chem. Soc. 2013, 135, 10124−10133

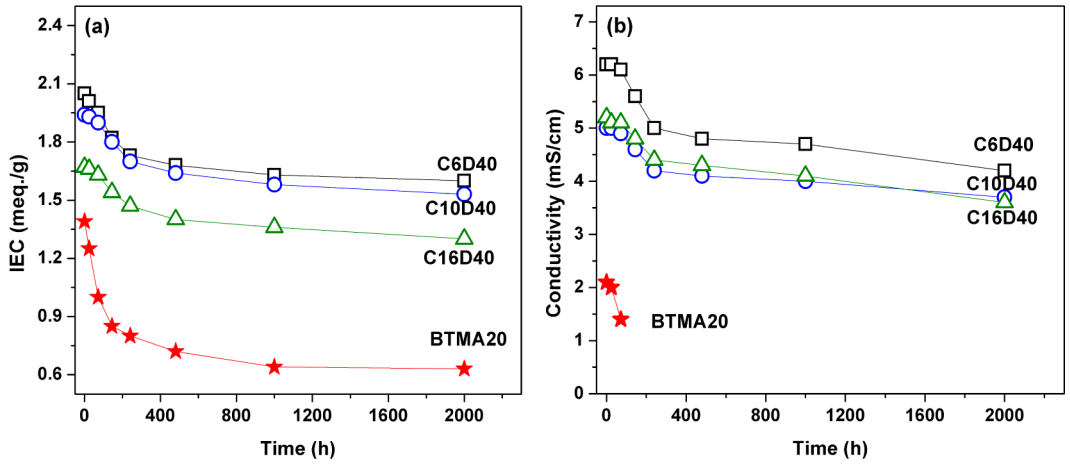

Figure 9. The changing trend in (a) IEC values and (b) bicarbonate of comb-shaped **CyDx** and **BTMAx** membranes after immersion in 1 M NaOH solution at 80 °C.

Scheme 2. Chemical Structures of 2C6Dx and 3C6Dx Having Two or Three Hexyl Side Chains

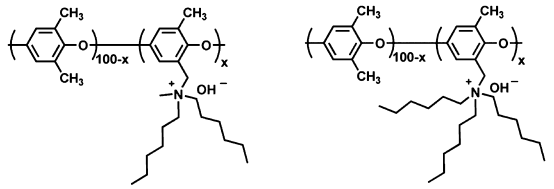

and expected to increase the hydrophobicity and volume which would possibly improve the hydrophilic−hydrophobic separation and strengthen the alkaline stability of the resulting materials. However, high IEC **3C6Dx** membranes could not be obtained from solution casting because of the immiscibility between the three large-volume alkyl chains and PPO backbone. Opaque **3C6D60** membrane with the IEC of 1.62 meq/g (measured by titration) was obtained. Although the multialkyl side chains-based **2C6Dx** and **3C6Dx** membranes displayed the similar comb-shaped structures and alkaline stability, low water uptake and conductivities resulted compared to **CyDx** membranes having only one side chain. As shown in Figure 10, the **C16D40** membranes with one

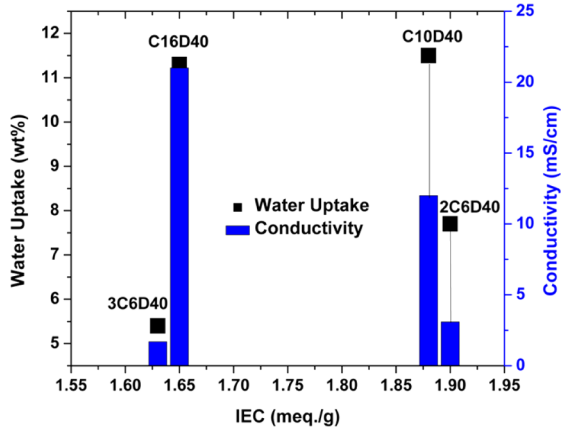

Figure 10. Comparison of the hydroxide conductivity and water uptake for **CyDx** with one alkyl side chain and the membranes (**2C6D40** and **3C6D40**) with multiple alkyl side chains.

hexadecyl side chain showed much higher water uptake of (12 wt %) and hydroxide conductivity (21 mS/cm) than that of **3C6D40** membranes having three hexyl side chains (WU = 5.4 wt %, σ = 1.7 mS/cm) despite their similar IEC value (~1.6 meq/g). These results suggest that multialkyl side chains on quaternary ammonium cationic centers are not helpful for the hydroxide transport in the membrane probably due to the high hydrophobicity of multialkyl chains.

Fuel Cell Performance. Although the comb-shaped copolymers have been shown to be highly ion-conductive and stable to high pH environments, the most practical evaluation of these materials is their performance in AMFC single cells as the ion-conductive material in the catalyst layer. We chose evaluation in a catalyst layer because the polymer is in intimate contact with the catalysts and experiences the most electrochemical stress in an operating device. We hypothesize that polymers that can have good performance and lifetime in the catalyst layers will also serve as good membranes. Figure 11a shows the polarization curves of an H_2/O_2 AEMFC with comb-shaped copolymers **C6D60** and **C16D40** as the ionomers in both the anode and cathode catalyst layers. The open circuit voltages (OCVs) are close to the theoretical value of about 1.1 V, indicating that the **CyDx** ionomers do not affect the catalyst function of Pt significantly. The peak power density for the AEMFC with the **C16D40** ionomer was 77 mW cm^{-2}, which was slightly higher than that of value with **C6D60** ionomer (67 mW cm^{-2}) under the same conditions in spite of the lower IEC values and hydroxide conductivity of **C16D40** ionomer. The data suggests that the phase separated structure of the **C16D40** sample as shown in SAXS may have helped to build a more efficient three-phase boundary in the catalyst layer. Additionally, the increased hydrophobicity imparted by the C16 chain compared to the C6 chain may have affected the water transport in the catalyst layer.[48,49] Furthermore, the fuel cell results in this work are much higher than the 22 mW cm^{-2} obtained for AEMFCs containing A3Ver2 ionomers and comparable to the value from AS-4 ionomers (95 mW cm^{-2})[49] and cross-linked ionomer (90 mW cm^{-2})[51] for AEMFCs. The measured high frequency resistance (0.6 Ω cm^2) was much smaller than the values of 1.0 Ω cm^2 observed for the AEMFCs with a cross-linked ionomer.[51] The higher power density and smaller internal resistance indicate that the comb-shaped **CyDx** is a promising ionomer that is soluble in

dx.doi.org/10.1021/ja403671u | J. Am. Chem. Soc. 2013, 135, 10124−10133

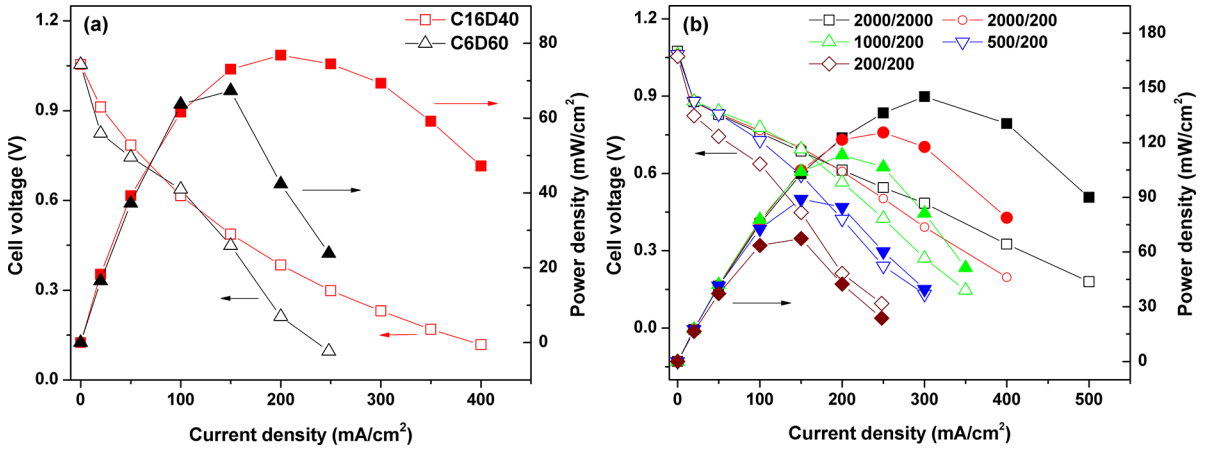

Figure 11. Polarization curves and power density curves of an AEMFC at 50 °C (a) with the **CyDx** ionomer with H_2/O_2 flow rate of 200/200 cm^3/min and (b) with the **C6D60** ionomer with different H_2/O_2 flow rates. Test conditions: catalyst loadings of 0.5−0.60 mg Pt/cm^2 and 0.270−0.325 mg **CyDx**/cm^2 for both anode and cathode, A201 commercial membrane, humidifier temperatures of 50 and 50 °C for H_2 and O_2, respectively.

low-boiling-point solvents for fuel cell processing but is insoluble during alkaline fuel cell operation.

Figure 11b shows the polarization curves of the **C6D60** containing AEMFC at different gas flow rates. The peak power density increased with flow rate, while the opposite trend was observed for the internal resistances. The highest peak power density was up to 145 mW cm^{-2} when the H_2/O_2 flow rate was 2000/2000 cm^3/min, which is much higher than the value obtained from crosslined electrochemical interface (90 mW cm^{-2}) under the same gas flow rate conditions.[51] At the same time, the internal resistance of 0.3 Ω cm^2 was also much smaller than the value of 2.3 Ω cm^2 obtained with a AEMFC using a cross-linked ionomer. The results demonstrate that comb-shaped **CyDx** ionomer is superior to other types of quaternary ammonium hydroxide ionomers. Although the **C16D40** ionomer-based alkaline fuel cell had better initial performance with higher peak power density, its durability (lifetime) in a single cell was only 12 h which could be attributed to the poor compatibility between long alkyl chain and polymer backbone causing mechanical failure of the electrode or the possible oxidative degradation the thin ionomer layer under fuel cell operating conditions where the steric shielding in the ionomer layer is not as effective as it is in the membrane.[13] On the contrary, the **C6D60** ionomer kept 90% of its initial performance after 60 h testing, as shown in Figure 12. Since the **C6D60** sample qualitatively had better mechanical properties in membrane samples than the **C16D40** sample and the membrane degradation of these samples was not greatly different, we might conclude that mechanical properties of the ionomer in the fuel cell electrode may play a role in device lifetime. Further device optimization studies are needed to optimize catalysts and MEA fabrication procedure to improve the compatibility between the interface of catalyst and ionomer.

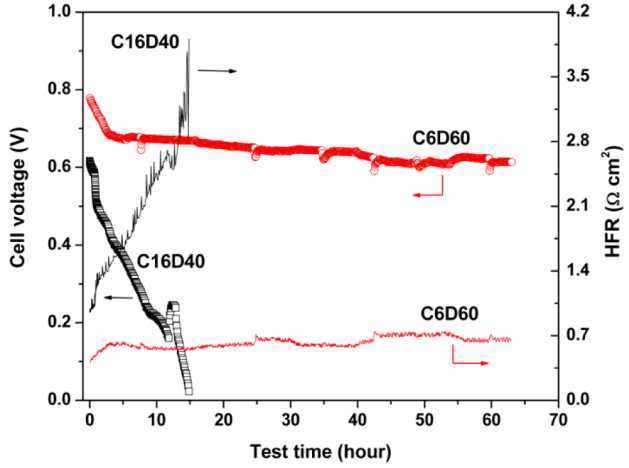

Figure 12. Lifetime test with **CyDx** ionomers in AMFCs. Test conditions: loadings of 0.5−0.6 mg Pt/cm^{-2} and 0.270−0.325 mg/cm^{-2} of **CyDx** ionomer for both anode and cathode; discharge current: 100 mA/cm^2, A201 commercial membrane, humidifier temperatures of 50 and 50 °C for H_2 and O_2, respectively.

CONCLUSION

In summary, we have designed and synthesized comb-shaped AEMs with one or multiple long alkyl side chains from C6 to C16 that provide multiple structural variations to allow tuning of the membrane properties. The comb-shaped copolymers with one alkyl side chain exhibited organized ionic domains that depended on the side chain length and resulted in an enhancement in hydroxide conductivity relative to other types of AEMs with multiple side chains or typical AEMs based on the benzyltrimethyl ammonium motif. The **CyD40** membranes have similar alkaline stability and were stable up to 2000 h in 1 M NaOH at 80 °C. The steric effects of the long alkyl chains surrounding the quaternary ammonium center are likely the cause of these materials' good alkaline stability. The **C16Dx** membranes having the longest hexadecyl chain showed better properties including lower water uptake, more distinct ionic domains, and higher hydroxide conductivity, compared to those of **C6Dx** membranes with a hexyl side chain. However, poor film-forming ability was observed with high IEC C16 materials which probably resulted from the poor compatibility between long alkyl side chain and polymer backbone. Thus, high IEC (up to 2.5 meq/g) membranes with one hexadecyl side chain were not obtained. Moreover, the **CyDx** samples had excellent solubility in low-boiling point, water-soluble solvents which make these materials interesting as AEMFCs ionomers. The H_2/O_2 AEMFC containing the **CyDx** ionomers exhibits an increase in peak power density and reduction of internal resistance compared to that in literature reports. Although the **C16D40** ionomer-based AEMFC showed slightly higher peak

dx.doi.org/10.1021/ja403671u | J. Am. Chem. Soc. 2013, 135, 10124−10133

power density, short lifetime was observed. The hexyl chain **C6D60** ionomer-based AEMFC retained 90% of its initial performance after 60 h. We consider that these comb-shaped copolymers could lead to new materials for the production of AEMs that meet the demanding challenges of alkaline fuel cells. The long alkyl chain platform is versatile because it can be prepared using a number of pendant substituents to the quaternary ammonium center, which may be further modified to address the various separations and energy-focused applications.

AUTHOR INFORMATION

Corresponding Author

hickner@matse.psu.edu

Notes

The authors declare no competing financial interest.

ACKNOWLEDGMENTS

This work was funded by the Advanced Research Projects Agency-Energy (ARPA-E), U.S. Department of Energy, under Award No. DE-AR0000121.

REFERENCES

(1) Appleby, A. J.; Foulkes, F. R. *Fuel Cell Handbook*; Van Nostrand Reinhold: New York, 1989.
(2) Carratte, L.; Friedlich, K. A.; Stimming, U. *Fuel Cells* **2001**, *1*, 5.
(3) Steele, B. C. H.; Heinzel, A. *Nature* **2001**, *414*, 345.
(4) Borup, R.; Meyers, J.; Pivovar, B.; Kim, Y. S.; Mukundan, R.; Garland, N.; Myers, D.; Wilson, M.; Garzon, F.; Wood, D.; Zelenay, P.; More, K.; Stroh, K.; Zawodzinski, T.; Boncella, J.; McGrath, J. E.; Inaba, M.; Miyatake, K.; Hori, M.; Ota, K.; Ogumi, K.; Miyata, S.; Nishikata, A.; Siroma, Z.; Uchimoto, Y.; Yasuda, K.; Kimijima, K.; Iwashita, N. *Chem. Rev.* **2007**, *107*, 3904−3951.
(5) Diat, O.; Gebel, G. *Nat. Mater.* **2008**, *7*, 13−14.
(6) Hickner, M. A.; Ghassemi, H.; Kim, Y. S.; Einsla, B. R.; McGrath, J. E. *Chem. Rev.* **2004**, *104*, 4587−4611.
(7) Eisenberg, A.; Yeager, H. L. *Perfluorinated Ionomer Membranes*; ACS Symposium Series *180*; American Chemical Society: Washington, DC, 1982.
(8) Tant, M. R.; Kauritz, K. A.; Wilkes, G. L. *Ionomers*; Chapman & Hall: UK, 1997.
(9) Varcoe, J. R.; Slade, R. C. T. *Fuel Cells* **2005**, *2*, 187−200.
(10) Xu, T. *J. Membr. Sci.* **2005**, *263*, 1−29.
(11) Hickner, M. A. *Mater. Today* **2010**, *13*, 34−41.
(12) Merle, G.; Wessling, M.; Nijmeijer, K. *J. Membr. Sci.* **2011**, *377*, 1−35.
(13) Pan, J.; Chen, C.; Zhuang, L.; Lu, J. *Acc. Chem. Res.* **2012**, *45*, 471−483.
(14) Wang, Y.; Qiao, J.; Baker, R.; Zhang, J. *Chem. Soc. Rev.* **2013**, DOI: 10.1039/C3CS60053J.
(15) Varcoe, J. R.; Slade, R. C. T.; Wright, G. L.; Chen, Y. L. *J. Phys. Chem. B* **2006**, *110*, 21041−21049.
(16) Wu, X.; Scott, K. *J. Power Sources* **2012**, *206*, 14−19.
(17) Asazawa, K.; Yamada, K.; Tanaka, H.; Oka, A.; Taniguchi, M.; Kobayashi, T. *Angew. Chem., Int. Ed.* **2007**, *46*, 8024−8027.
(18) Tanaka, M.; Fukasawa, K.; Nishino, E.; Yamaguchi, S.; Yamada, K.; Tanaka, H.; Bae, B.; Miyatake, K.; Watanabe, M. *J. Am. Chem. Soc.* **2011**, *133*, 10646−10654.
(19) Yan, J.; Hickner, M. A. *Macromolecules* **2010**, *43*, 2349−2356.
(20) Hibbs, M. R.; Hickner, M. A.; Alam, T. M.; McIntyre, S. K.; Fujimoto, C. H.; Cornelius, C. J. *Chem. Mater.* **2008**, *20*, 2566−2573.
(21) Wang, J.; Li, S.; Zhang, S. *Macromolecules* **2010**, *43*, 3890−3896.
(22) Kim, D. S.; Labouriau, A.; Guiver, M. D.; Kim, Y. S. *Chem. Mater.* **2011**, *23*, 3795−3797.
(23) Zhang, Q.; Li, S.; Zhang, S. *Chem. Commun.* **2010**, *46*, 7495−7497.
(24) Gu, S.; Cai, R.; Luo, T.; Chen, Z.; Sun, M.; Liu, Y.; He, G.; Yan, Y. *Angew. Chem., Int. Ed.* **2009**, *48*, 6499−6502.
(25) Robertson, N. J.; Kostalik, H. A., IV; Clark, T. J.; Mutolo, P. F.; Abruna, H. D.; Coates, G. W. *J. Am. Chem. Soc.* **2010**, *132*, 3400−3404.
(26) Varcoe, J. R.; Slade, R. C. T.; Yee, E. L. H.; Poynton, S. D.; Driscoll, D. J.; Apperley, D. C. *Chem. Mater.* **2007**, *19*, 2686−2693.
(27) Zeng, Q. H.; Liu, Q. L.; Broadwell, I.; Zhu, A. M.; Xiong, Y.; Tu, X. P. *J. Membr. Sci.* **2010**, *349*, 237−243.
(28) Luo, Y.; Guo, J.; Wang, C.; Chu, D. *J. Power Sources* **2010**, *195*, 3765−3771.
(29) Wu, L.; Zhou, G.; Liu, X.; Zhang, Z. H.; Li, C.; Xu, T. *J. Membr. Sci.* **2011**, *371*, 155−162.
(30) Li, N.; Yan, T.; Li, Z.; Thurn-Albrecht, T.; Binder, W. H. *Energy Environ. Sci.* **2012**, *5*, 7888−7892.
(31) Hibbs, M. R.; Fujimoto, C. H.; Cornelius, C. J. *Macromolecules* **2009**, *42*, 8316−8321.
(32) Hinksman, P.; Isaac, D. H.; Morrissey, P. *Polym. Degrad. Stab.* **2000**, *68*, 299−305.
(33) Zha, Y.; Disabb-Miller, M. L.; Johnson, Z. D.; Hickner, M. A.; Tew, G. N. *J. Am. Chem. Soc.* **2012**, *134*, 4493−4496.
(34) Thomas, O. D.; Soo, K. J. W. Y.; Peckham, T. J.; Kulkarni, M. P.; Holdcroft, S. *J. Am. Chem. Soc.* **2012**, *134*, 10753−10756.
(35) Noonan, K. J. T.; Hugar, K. M.; Kostalik, H. A.; Lobkovsky, E. B.; Abruna, H. D.; Geoffrey W. Coates, G. W. *J. Am. Chem. Soc.* **2012**, *134*, 18161−18164.
(36) Deavin, O. I.; Murphy, S.; Ong, A. L.; Poynton, S. D.; Zeng, R.; Herman, H.; Varcoe, J. R. *Energy Environ. Sci.* **2012**, *5*, 8584−8597.
(37) Arges, C. G.; Ramani, V. *Proc. Natl. Acad. Sci. U.S.A.* **2013**, *110*, 2490−2495.
(38) Fujimoto, C.; Kim, D. S.; Hibbs, M.; Wrobleski, D.; Kim, Y. S. *J. Membr. Sci.* **2012**, *423*−*424*, 438−449.
(39) Chempath, S.; Boncella, J. M.; Pratt, L. R.; Henson, N.; Pivovar, B. S. *J. Phys. Chem. C* **2010**, *114*, 11977−11983.
(40) Tomoi, M.; Yamaguchi, K.; Ando, R.; Kantake, Y.; Aosaki, Y.; Kubota, H. *J. Appl. Polym. Sci.* **1997**, *64*, 1161−1167.
(41) Hibbs, M. R. *J. Polym. Sci., Part B: Polym. Phys.* **2012**, DOI: 10.1002/polb.23149.
(42) Kim, Y. S.; Einsla, B.; Sankir, M.; Harrison, W.; Pivovar, B. S. *Polymer* **2006**, *47*, 4026−4035.
(43) Roy, A.; Hickner, M. A.; Yu, X.; Li, Y.; Glass, T. E.; McGrath, J. E. *J. Polym. Sci., Part B: Polym. Phys.* **2006**, *44*, 2226−2239.
(44) Elabd, Y. A.; Hickner, M. A. *Macromolecules* **2011**, *44*, 1−11.
(45) Adams, L. A.; Poynton, S. D.; Tamain, C.; Slade, R. C. T.; Varcoe, J. R. *ChemSusChem* **2008**, *1*, 79−81.
(46) Unlu, M.; Zhou, J.; Kohl, P. A. *Electrochem. Solid-State Lett.* **2009**, *12*, B27−B30.
(47) Chen, D.; Hickner, M. A. *ACS Appl. Mater. Interfaces* **2012**, *4*, 5775−5781.
(48) Gu, S.; Skovgard, J.; Yan, Y. S. *ChemSusChem* **2012**, *5*, 843−848.
(49) Murat Unlu, M.; Abbott, D.; Ramaswamy, N.; Ren, X.; Mukerjee, S.; Kohla, P. A. *J. Electrochem. Soc.* **2011**, *158*, B1423−B1431.
(50) Yanagi, H.; Fukuta, K. *ECS Trans.* **2008**, *16*, 257−262.
(51) Varcoe, J. R.; Slade, R. C. T. *Electrochem. Commun.* **2006**, *8*, 839−843.